Monthly Notices
of the
ROYAL ASTRONOMICAL SOCIETY

MNRAS **442,** 1142–1150 (2014) doi:10.1093/mnras/stu941

Visible near-diffraction-limited lucky imaging with full-sky laser-assisted adaptive optics

A. G. Basden★

Department of Physics, Durham University, South Road, Durham, DH1 3LE, UK

Accepted 2014 May 7. Received 2014 May 7; in original form 2014 April 7

ABSTRACT

Both lucky imaging techniques and adaptive optics require natural guide stars, limiting sky-coverage, even when laser guide stars are used. Lucky imaging techniques become less successful on larger telescopes unless adaptive optics is used, as the fraction of images obtained with well-behaved turbulence across the whole telescope pupil becomes vanishingly small. Here, we introduce a technique combining lucky imaging techniques with tomographic laser guide star adaptive optics systems on large telescopes. This technique does not require any natural guide star for the adaptive optics, and hence offers full sky-coverage adaptive optics correction. In addition, we introduce a new method for lucky image selection based on residual wavefront phase measurements from the adaptive optics wavefront sensors. We perform Monte Carlo modelling of this technique, and demonstrate *I*-band Strehl ratios of up to 35 per cent in 0.7 arcsec mean seeing conditions with 0.5 m deformable mirror pitch and full adaptive optics sky-coverage. We show that this technique is suitable for use with lucky imaging reference stars as faint as magnitude 18, and fainter if more advanced image selection and centring techniques are used.

Key words: instrumentation: adaptive optics – instrumentation: high angular resolution – methods: numerical – techniques: image processing.

1 INTRODUCTION

1.1 The quest for high-resolution optical astronomical images: adaptive optics and lucky imaging

The lucky imaging concept (Fried 1978), where selected short-exposure images are integrated into a final image using some selection criteria, is now an accepted technique in astronomy. This concept relies on utilizing the rare moments when perturbations introduced by atmospheric turbulence are minimal, to build up visible wavelength astronomical images. The criteria for image selection (i.e. which images to keep for integration, and which to discard) are a topic of active research (Staley et al. 2010; Garrel, Guyon & Baudoz 2012; Mackay 2013). However, all rely on having one or more selection stars (guide stars) within the field of view. These guide stars are used to determine whether the selection criterion has been met. These stars must be sufficiently bright to ensure that the selection criteria can be measured within the short atmospheric coherence time, and therefore, sky-coverage is somewhat restricted (Tubbs et al. 2002).

Lucky imaging works well on 1–2 m class telescopes, where there is a significant chance of the perturbed wavefront being instantaneously flat over the whole telescope aperture. However, on larger telescopes, the probability of the atmospheric turbulence producing a flat wavefront over the whole telescope pupil (and hence, a lucky image) is significantly reduced, with returns reducing as telescope size increases.

Adaptive optics (AO; Babcock 1953) is a technique used to detect time varying optical perturbations and correct for them in real-time. Widely used in astronomy, AO has led to a breakthrough in ground-based infrared astronomical imaging, with near-diffraction-limited images routinely produced. However, AO performance at visible wavelengths is poorer, with images being far from diffraction limited, though somewhat improved over uncorrected, seeing-limited images. A combination of AO with lucky imaging has been proposed and implemented (Femenia et al. 2011; Mackay et al. 2012) with impressive results. However, AO also brings a requirement for sufficiently bright guide star targets to be used for wavefront sensing, again with sky-coverage implications. The use of laser guide stars (LGSs; Foy & Labeyrie 1985) with lucky imaging has been proposed (Law et al. 2008), with the LGSs leading to improved sky-coverage. Unfortunately, even these systems require at least one sufficiently bright natural guide star (NGS) to overcome the LGS tip–tilt ambiguity.

Here, we introduce a concept for lucky imaging assisted by AO where AO sky-coverage is unlimited. We propose to use multiple LGSs to perform tomographic reconstruction of the atmosphere,

★E-mail: a.g.basden@durham.ac.uk

as is done by wide-field AO systems (Myers et al. 2008). This technique uses no NGSs and so the reconstructed atmospheric phase contains an unknown tip–tilt component, translating to an image shift in the telescope focal plane. The AO-corrected lucky images are then selected, either using conventional methods, or using wavefront phase information, a technique which we introduce and describe here. Finally, recentring of the selected lucky images is performed.

In Section 2, a description of these techniques is given, along with the details of modelling and simulations performed. In Section 3, we discuss simulation results and implications. In Section 4, we discuss plans for on-sky testing and we conclude in Section 5.

2 LGS-ASSISTED LUCKY IMAGING

A tomographic (3D) reconstruction of atmospheric turbulence is possible when multiple guide stars are available (Assémat, Gendron & Hammer 2007). By correlating wavefront sensor measurements corresponding to different source directions, the height of the perturbations introduced by the atmosphere can be determined, and a corresponding mitigation can be applied. A requirement for many NGSs has sky-coverage implications. However, multiple LGS AO systems have recently come online (Morris et al. 2012), allowing tomographic reconstruction to be performed with only one NGS (which is required to determine the global tip–tilt, to which LGSs are insensitive).

2.1 Using wavefront phase for image selection

A projection of the reconstructed turbulent volume along any given line of sight allows the perturbed wavefront incident from any direction within the field of view to be estimated, as has been successfully demonstrated by multi-object AO (MOAO) systems (Assémat et al. 2007; Basden et al. 2013). This information can then be used as a criterion for lucky image selection. If the root-mean-square (rms) wavefront error is below a particular value at a given instant in time, then the corresponding lucky image should be used rather than discarded. This has an advantage over traditional means of image selection in that since the perturbed wavefront can be estimated over the entire field of view, it is now possible to select only parts of this field for integration, while discarding parts where wavefront perturbation is higher.

2.1.1 LGS tip–tilt measurement

If LGS information is used to compute the selection criteria metric for lucky imaging as previously described, the unknown tip–tilt component (due to the lack of NGS information) manifests itself as common lateral movement of objects in the image plane. Therefore, individually selected lucky images can simply be shifted and added. However, unless taken into account, this unknown wavefront tilt will affect the selection criteria, which are based on wavefront error, since rms wavefront error increases with wavefront tilt. Therefore, it is necessary to remove the tip and tilt components from the reconstructed wavefronts before using them to determine whether the image selection criteria have been met. In other words, using LGS tomography, a selection criteria for lucky images can be obtained, based on the rms of tilt-removed reconstructed wavefront phase in any given source direction.

These selected images can then be shifted and added, with the shift determined either from a NGS, or from information within the lucky image itself, for example, the centroid location of a bright star or Fourier information across the whole image (since the tip–tilt can be assumed to be global over a few tens of arcsec). In the case where selection criteria are based on wavefront error from the LGSs, it should be noted that since image selection is not performed using the individual lucky images, reduced photon flux within these images may be acceptable, as we will show in following sections. It should also be noted that centroiding of any lucky images requires enough light within the images in the field to be present, and that this is generally not effective on diffuse objects such as galaxy images.

2.2 Wavefront correction with a deformable mirror

AO entails the correction of a wavefront using a deformable mirror (DM). This can be combined with lucky imaging for improved performance (Mackay et al. 2012). The combination of lucky imaging with a single LGS AO system has also been suggested and demonstrated (Law et al. 2008). However, in this case, the lucky image selection criteria were determined from the lucky images, and an NGS was required to avoid tip–tilt ambiguity for the AO correction, and thus sky-coverage was limited.

This NGS requirement is however not necessary if the AO correction is aiming to only sharpen each individual lucky image rather than the mean long exposure image. In this case, using multiple LGSs such that the turbulent volume is well sampled, an AO correction can be computed with the tip/tilt component present, but ignored. The corrected AO image will then have an undetermined instantaneous tip and tilt (position shift in the image plane), but be otherwise relatively well corrected. The selected lucky images (using either the wavefront phase criterion estimated from LGS information, or conventional image selection techniques) can then be shifted and added, with the shift determined using the information within the lucky image (i.e. light from all sources within limits defined by the field of view or the tip–tilt isoplanatic patch size). It should be noted that markedly poorer resolution can be obtained if image recentring on multiple targets is not performed with care, essentially due to tip–tilt anisoplanatism, causing radial scale variations.

If the LGSs are operating in open-loop, i.e. are insensitive to changes to the DM surface (as in the case of an MOAO system such as CANARY), then there is a degree of flexibility in the mode of AO correction that is performed, including MOAO (if several DMs are available), laser tomographic adaptive optics (LTAO, to correct a single line of sight) and ground layer adaptive optics (GLAO, to perform moderate correction over a wide field of view).

2.2.1 Estimation of open-loop AO-corrected image phase

If the LGSs are operating in open-loop, then the estimated wavefront phase will not be equal to that seen by the lucky imaging detector, since this is placed after the DM. However, as we will show, it is still possible to use the reconstructed phase to derive the lucky image selection criterion.

2.3 Modelling of LGS assisted lucky imaging

We have used the Durham AO simulation platform (Basden et al. 2007; Basden, Myers & Butterley 2010a) to perform full end-to-end Monte Carlo simulation of LGS-assisted lucky imaging, and here describe our model. This is based loosely around the CANARY instrument, since we intend to use this instrument for on-sky testing

of the concepts described in this paper. We assume a 4.2 m telescope with a 1.2 m central obscuration (representative of the William Herschel Telescope). We use four Rayleigh LGSs at 22 km, placed in a circular asterism with a 40 arcsec diameter, and cone effect, spot elongation and laser uplink effects are included in our simulations. A 532 nm wavelength is assumed for the LGS. For comparison, we also show results when sodium LGSs are used, with the sodium beacon at 90 km.

When performing AO correction, the DM is operated in open-loop (i.e. not sensed by the wavefront sensors). We vary the number of sub-apertures between 8×8 (the default case) and 32×32, with 4 pixels per sub-aperture, and a pixel scale of 0.84 arcsec pixel^{-1}. We model a DM with 5×5 and 9×9 actuators, with 9×9 being the default case (which is to be assumed unless stated otherwise). We use a nine layer atmospheric profile (Basden et al. 2013) with a 20 m outer scale and a Fried's parameter, $r_0 = 13.5$ cm, corresponding to 0.8 arcsec seeing, unless otherwise stated. The simulation time-step is 2.5 ms, the WFS exposure time is 5 ms (2 simulation time-steps) and the lucky image exposure time is 10 ms (4 simulation time-steps). We simulate 250 s of telescope time for each case that is considered.

We ignore the mean tip–tilt component of each LGS when reconstructing wavefront phase perturbations, and do not use any additional tip–tilt information, i.e. tip–tilt remains uncorrected. Wavefront reconstruction is performed by placing virtual DMs at each turbulent layer, and using a minimum variance reconstruction formulation (Ellerbroek, Gilles & Vogel 2003) to derive the corresponding wavefront phase. We then propagate the tomographically reconstructed wavefront phase along a given line of sight to estimate the wavefront perturbation in that particular direction.

Fig. 1 shows the LGS pupil overlap at the heights of four atmospheric layers: tomographic reconstruction of wavefront phase is theoretically possible whenever two guide star pupils overlap, and therefore, the 90 km case provides better coverage of tomographic phase information.

The lucky images are generated assuming a detector with 256×256 pixels and a field of view of 5 arcsec for each line of sight. The angular resolution of the telescope at the 800 nm wavelength used is about 0.05 arcsec We consider lucky images for sources up to one arcmin off-axis, with on-axis results being presented by default. These images are considered to have high signal-to-noise ratio (no noise) unless otherwise stated.

We assume idealized telescope tracking and stability, and that there the non-common path errors between the AO system and the lucky imaging system have been removed. We also assume that the telescope is well focused. Real telescope operational parameters will result in slight performance degradation, particularly when operating without the AO loop. This will be of particular importance when there are high-frequency vibration modes within the telescope structure, at frequencies approaching that of the lucky imaging system frame rate. However, on the William Herschel Telescope (WHT), we have identified the highest frequency vibration with significant power at 22 Hz (Sivo et al. 2014), which will have negligible impact on individual lucky image quality, and can be corrected using vibration control techniques, such as a Kalman filter, as we have demonstrated (Sivo et al. 2014). However, the effect of these assumptions should be borne in mind.

2.3.1 *Variation of* r_0

When used on-sky, lucky imaging takes advantage of the fact that the instantaneous atmospheric Fried's parameter, r_0, is not constant.

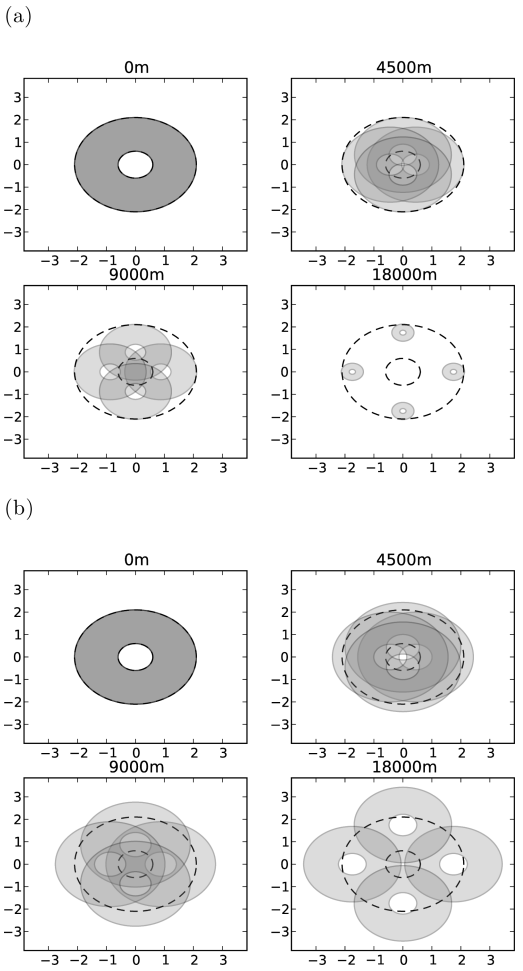

Figure 1. LGS pupil overlap at different heights (shown in the titles) above the telescope. (a) For Rayleigh LGS focused at 22 km. (b) For sodium LGS focused at 90 km.

Therefore, at times when r_0 is large, good images are collected, while when r_0 is smaller, more images are thrown away. In our simulations, we usually assume that r_0 is constant, meaning that our results will be somewhat pessimistic. We do, however, provide results from simulations performed with different values of r_0. Additionally, we also include results from simulations where the value of r_0 is changing throughout the simulation period.

2.4 Lucky selection criteria

For comparative purposes, we use selection criteria derived from the lucky images themselves, and from the tomographically projected (along each line of sight of interest) tilt-removed rms wavefront perturbation (with flatter wavefronts producing cleaner point spread functions (PSFs)).

Selection criteria derived from the lucky images themselves include Strehl ratio and diameter encompassing 50 per cent of image energy. It should be noted that using a Strehl ratio selection criterion introduces a performance bias when Strehl ratio is also used to determine final image quality, leading to overestimation of performance, particularly at low signal levels when noise can have a large effect on measured instantaneous Strehl ratio. However, we find it useful to include these results nevertheless, as image selection by Strehl ratio is conceptually easy to understand.

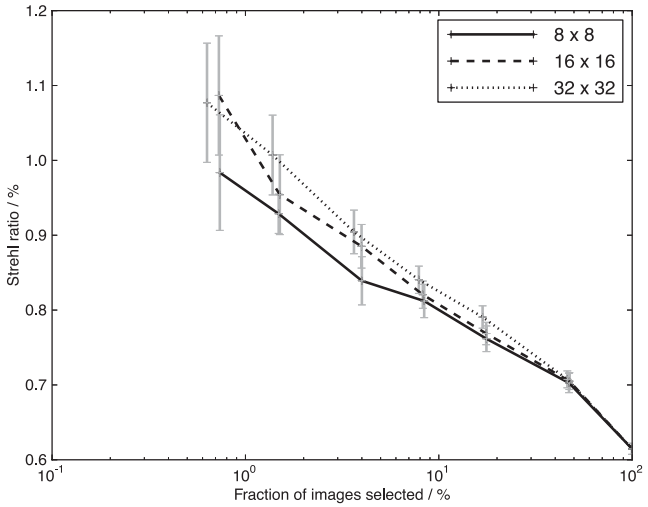

Figure 2. Lucky image quality (Strehl ratio) as a function of fraction of images selected. The solid curve represents selection using 8 × 8 sub-aperture WFSs, the dashed curve is for 16 × 16 sub-apertures and the dotted curve is for 32 × 32 sub-apertures. No AO correction is performed.

2.5 Shift and adding images

Since the LGS do not measure, and cannot correct, mean image position, we have to recentre the selected lucky images before summation. There are many ways to do this in the literature (Mackay 2013). Here, we simply measure the image centre of gravity, and shift the image by a whole number of pixels. Although this is not optimal, it maintains simplicity in our results.

The final images (comprising many shifted and added selected lucky images) are then processed to compute Strehl ratio, full width at half-maximum and diameter encircling 50 per cent of energy. We do not consider any Fourier-based image selection techniques here.

3 PERFORMANCE OF LGS-ASSISTED LUCKY IMAGING

We consider first the case where no AO correction is performed, to investigate the LGS wavefront phase-based selection criteria. Here, we use the LGSs to tomographically compute wavefront phase along a given line of sight, and the lucky image selection criteria are derived from the rms wavefront phase. Fig. 2 shows on-axis lucky image quality as a function of fraction of images selected, for different WFS orders (number of sub-apertures), which are used to obtain the lucky image selection criteria. It should be noted that no AO correction is performed, i.e. the LGSs are used for wavefront measurement only. As expected, the image quality is reduced as a greater fraction of images are selected. It can also be seen that using a higher order WFS generally gives a better image selection measurement, as would be expected due to the increased detail in reconstructed phase. The uncorrected, long-exposure Strehl ratio in this case is about 0.5 per cent, and therefore a factor of 2 improvement can be achieved.

3.1 AO correction using LGS measurements

We now consider the case where AO correction is performed, using a DM, the surface of which is shaped using the LGS WFS measurements. As detailed in the previous section, the mean LGS tip–tilt signal from each LGS is ignored, such that the AO correction improves the instantaneous PSF, but this is not in a fixed location.

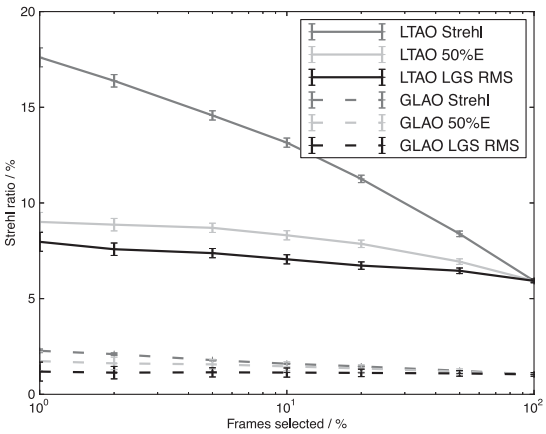

Figure 3. Integrated lucky image quality as a function of fraction of frames selected, for selection criteria based on LGS rms wavefront error, on image Strehl ratio and on PSF diameter encircling 50 per cent of energy (50 % E). Cases using both an LTAO correction and a GLAO correction are shown (both without global tip/tilt correction).

Therefore, shifting and adding of selected lucky images is still required. We consider the case where a tomographic GLAO correction is performed (i.e. the DM is used only to correct ground layer turbulence), and also where an LTAO correction is performed (i.e. the tomographic wavefront estimate is projected along the on-axis line of sight). Fig. 3 shows that LTAO correction offers significant performance benefits for on-axis lucky imaging over a global GLAO correction. This also shows that lucky image selection using LGS wavefront rms leads to poorer integrated images than when Strehl ratio is used as the selection criteria, though it does lead to some image quality improvement. Using PSF diameter as the lucky selection criteria gives performance close to that obtained using rms LGS wavefront error.

3.1.1 Open-loop WFS selection criteria

In the simulations presented here, our WFSs are operating in open-loop, so that they are insensitive to DM changes. Therefore, the selection criteria based on reconstructed phase require adjustment so that the DM correction is taken into account. We achieve this by computing the pseudo-closed-loop WFS signals, and using these to compute residual (corrected) phase, and hence selection criteria.

As shown in Fig. 4, there is a high degree of correlation between the computed residual wavefront phase rms and the open-loop-uncorrected wavefront phase rms, though with a residual rms having a consistently lower value (due to removal of lower order turbulent modes by the DM). It is therefore sufficient to use the open-loop-reconstructed wavefront phase rms as the lucky image selection criteria since a constant offset in criteria does not affect the images selected (we select a constant fraction).

3.1.2 LGS-assisted lucky imaging performance

Fig. 5(a) shows lucky image quality as a function of fraction of images selected, for selection criteria based on reconstructed wavefront. We consider several cases for WFS and DM order, and the uncorrected case (without AO) is shown for comparison. It should be noted that a higher WFS order does not necessarily lead to better image selection, as using 16 × 16 sub-apertures gives a similar final image Strehl ratio to 32 × 32 sub-apertures (since a DM with fewer

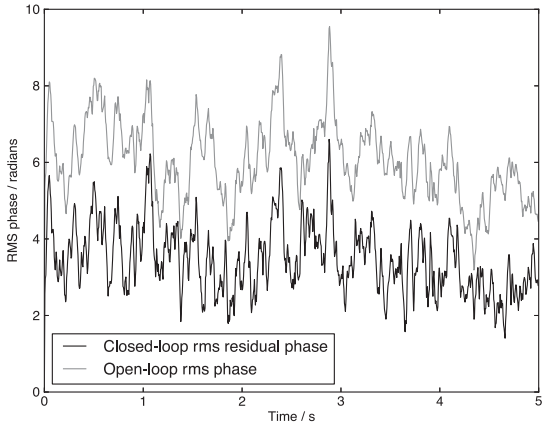

Figure 4. The rms-reconstructed tip–tilt removed wavefront phase as a function of time using open-loop WFSs, and pseudo-closed-loop WFSs.

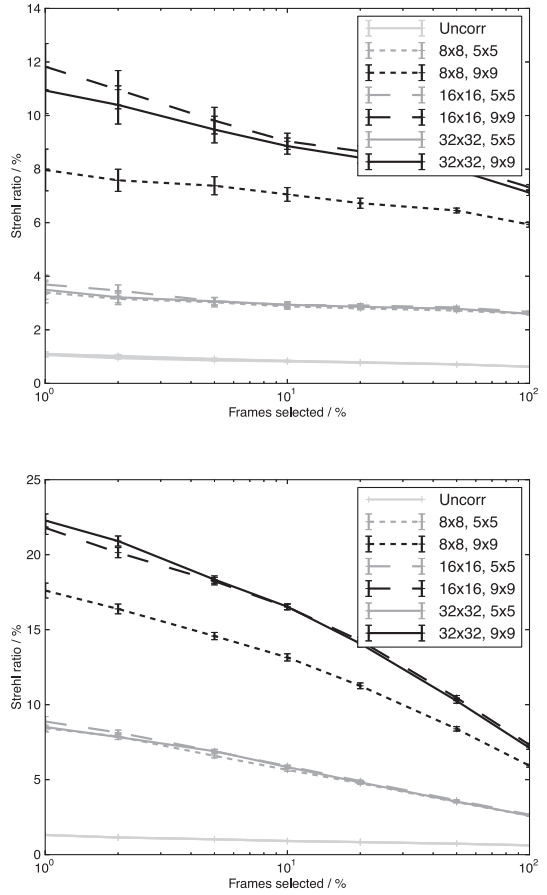

Figure 5. (a) Lucky image quality as a function of fraction of images selected, comparing different WFS and DM order as given in the legend (an even number of WFS sub-apertures, and an odd number of DM actuators). Uncorrected (no AO) performance is shown for comparison, and is relatively independent of WFS order (three cases are shown, but overlap, and hence only a single legend entry is given). (b) As for (a), but with the lucky image selection criteria derived from the short exposure Strehl ratios.

actuators is used), i.e. it is not necessary to significantly oversample the WFS with respect to the DM, though some oversampling does improve AO correction (when flux is not limited), as shown by the 16 × 16 sub-aperture case giving better performance than the 8 × 8 sub-aperture case.

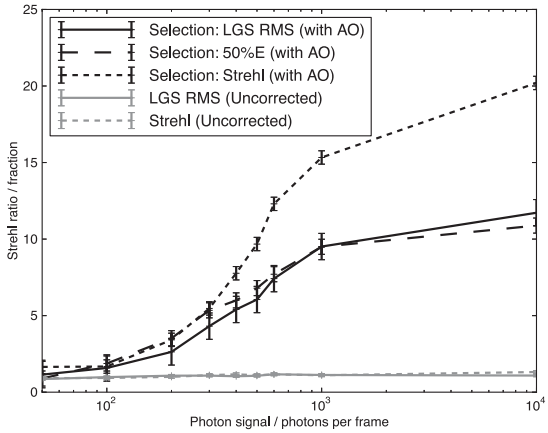

Figure 6. Lucky image quality as a function of detected signal level for selection criteria derived from rms wavefront and from individual image Strehl ratio, for a detector with 0.1 electrons readout noise.

Fig. 5(b) shows improved lucky image quality when lucky image Strehl ratio is used as the image selection criteria, and when the WFS order is increased above the DM order. This represents the extra information available during wavefront reconstruction being used to perform better AO correction.

3.1.3 Lucky image noise considerations

We now consider the case where noise is present within the lucky images, investigating a range of signal levels and readout noise. Lucky images are usually captured on flux-limited targets (due to the necessity for high frame rate), using low light level detectors, with photon counting strategies (Basden, Haniff & Mackay 2003). This has two effects. In the case where the image selection criteria are derived from the lucky image, the noise will affect the accuracy of image selection. Additionally, the noise will affect the accuracy of mean tip–tilt calculation (which is taken from the image) when shifting and adding the selected images.

We introduce photon shot noise, and also detector readout noise of both 0.1 electrons (corresponding to an electron multiplying CCD (EMCCD)) and 1 electrons (corresponding to an sCMOS detector), for the lucky imaging detectors. In the results that we present, it should be noted that we do not take detector quantum efficiency into account, nor the excess noise factor that affects EMCCD technologies (effectively halving quantum efficiency). Rather, we present results with detected signal level, giving the reader the freedom to scale these to incident flux depending on situation.

Fig. 6 shows lucky image quality as a function of signal level (in detected photons per lucky image frame), for image selection based both on the LGS signal and on lucky image characteristics (Strehl ratio and PSF diameter encircling 50 per cent energy). It can be seen that using image Strehl as the selection criteria gives better performance at all light levels.

Many science cases require images defined by criteria other than Strehl ratio, including for example ensquared energy within some box size (usually for a spectrograph), or the PSF diameter encircling some fraction of the available energy. Fig. 7 shows lucky image quality based on PSF diameter encircling 50 per cent of available energy, for different detector readout noise, using rms wavefront (from the LGS), lucky image Strehl ratio and PSF diameter as selection criteria. It can be seen here that at lower light levels, using the LGS rms wavefront as a selection criteria gives better

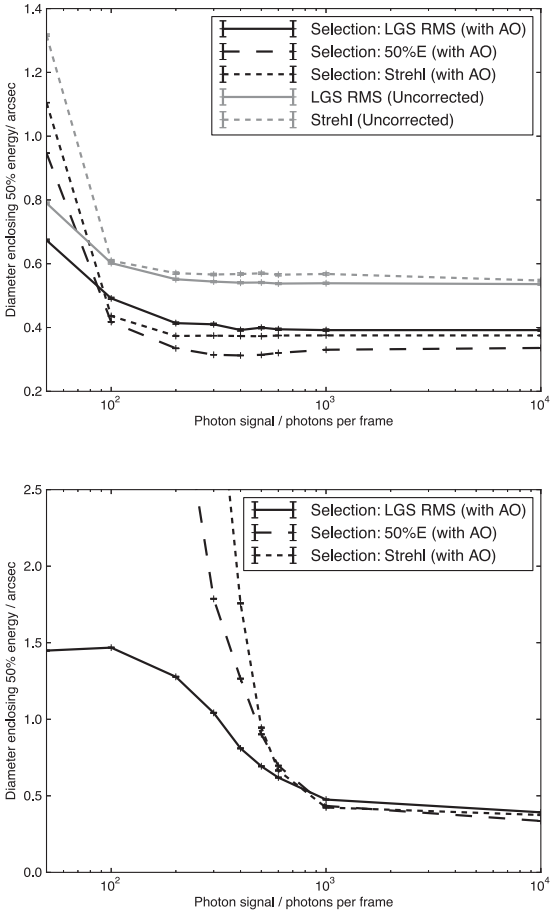

Figure 7. Integrated lucky PSF image diameter encircling 50 per cent of energy as a function of detected signal level for selection criteria derived from rms wavefront and from individual image Strehl ratio. A smaller diameter represents better performance. (a) For a detector with 0.1 electrons readout noise. (b) For a detector with 1 electron readout noise.

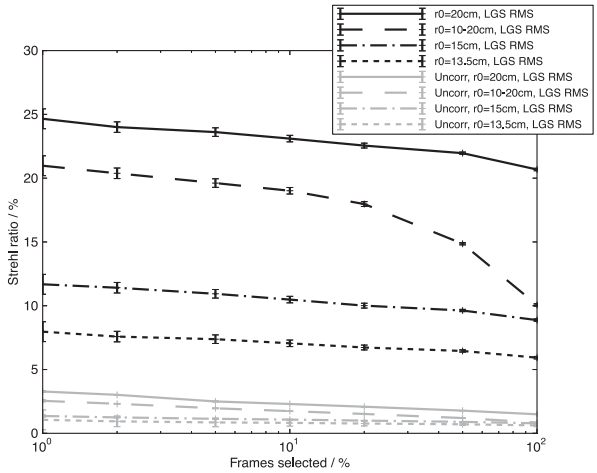

Figure 8. Lucky image quality as a function of fraction of images selected for different atmospheric Fried's parameters as given in the legend, with rms wavefront phase used for image selection. The AO-corrected and non-corrected cases are both shown (with 'Uncorr' in the legend representing the uncorrected cases).

performance than selection using the lucky images. The reason for this is that at these light levels, the estimated Strehl ratio will be affected significantly by photon shot noise and readout noise, which will significantly increase the probability of erroneous image selection. When considering Strehl ratio as the final image quality metric, this erroneous selection will have less of an effect than when other metrics, such as encircled energy diameter, are used. For the case of Strehl ratio, a bright pixel (amplified for example by unlikely Poisson or Gaussian statistics) will be identified as corresponding to a high Strehl ratio, and thus be selected. This lucky image will then be recentred and the bright pixel will improve Strehl of the final image. However, this instantaneous image could well have a broad PSF, with a wide energy spread, which will increase PSF diameter, resulting in poorer image quality, even though Strehl ratio is (spuriously) higher. It is therefore necessary, in the case of low photon flux, to consider carefully the metric used to measure image quality.

From Fig. 6, it can be seen that there is little performance improvement once signal levels reach about 1000 detected photons per lucky image frame. This corresponds to an *I*-mag 15 star on a 4.2 m telescope with a 100 Hz frame rate (Bessell 1979). Likewise, Fig. 7(a) shows that only 100 photons per lucky image (with a readout noise of 0.1 electrons) are required before little additional performance improvements is gained in the case when the integrated image quality metric is PSF diameter, corresponding to an *I*-mag 18 star. The presence of additional stars within the field of view would allow further improvements to be made, as would more advanced image selection and centring approaches, though we do not discuss this further here, rather relying on a simple centre-of-gravity calculation for image recentring.

3.2 Performance with different r_0

As previously discussed, lucky imaging relies on rapid variability of r_0 to work well, using images selected when r_0 is larger. We now consider four different situations in our simulations: constant values of r_0 of 13.5, 15 and 20 cm, and when r_0 varies sinusoidally from 10 to 20 cm with a 12.5 s period (corresponding to a mean r_0 of 15 cm for a 250 s simulation).

Fig. 8 shows lucky image quality as a function of image selection fraction for these different cases, when the selection criteria are derived from rms LGS wavefront error. As expected, a larger value of r_0 results in better performance. It can also be seen that in the case of a varying r_0, good performance is obtained when selection fraction is low (since the instantaneous images selected are generally those obtained during periods of high r_0), while image quality falls rapidly when the fraction of selected images is increased, since short exposure images captured during worse seeing conditions then have to be used. This shows that simulations of lucky imaging which use a constant r_0 value will be pessimistic. Corresponding uncorrected, long-exposure Strehl ratios are 1.2 (20 cm r_0), 0.71 (Variable r_0), 0.62 (15 cm r_0) and 0.5 per cent (13.5 cm r_0).

Lucky image quality when using a Strehl ratio criteria for image selection also depends (as expected) on r_0. Fig. 9 shows a comparison of different atmospheric conditions when lucky image Strehl ratio is used for image selection, and again shows image quality falling more rapidly with selection fraction when seeing is variable. *I*-band Strehl ratios of 35 per cent have been achieved with mean 15 cm r_0. Using the PSF diameter encircling 50 per cent energy as selection criteria leads to similar trends, though with lower final Strehl ratio, as shown in Fig. 10.

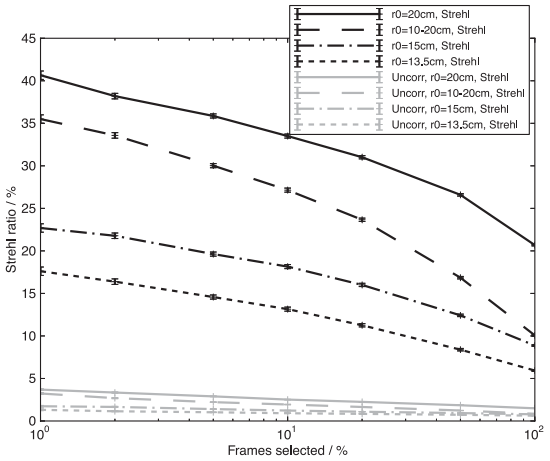

Figure 9. Lucky image quality as a function of fraction of images selected for different atmospheric Fried's parameters as given in the legend, with Strehl ratio used for image selection. The AO corrected and non-corrected are shown, with 'Uncorr' representing the uncorrected cases.

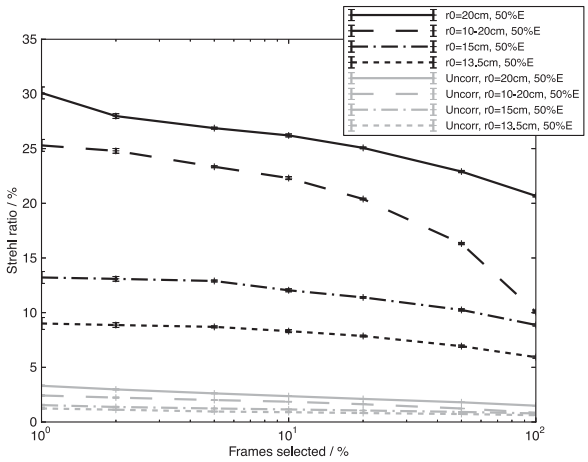

Figure 10. Lucky image quality as a function of fraction of images selected for different atmospheric Fried's parameters as given in the legend, with the diameter encircling 50 per cent PSF energy used for image selection. The AO corrected and non-corrected are shown, with 'Uncorr' representing the uncorrected cases.

3.3 Performance with sodium LGSs

Although we will be performing on-sky demonstration of this technique using Rayleigh LGSs, we have also investigated performance when using sodium LGSs, using a sodium layer profile centred at 90 km above the telescope. As shown in Fig. 1, increased LGS height results in increased sampling of the atmospheric turbulence, thus leading to better wavefront estimation and AO correction. Fig. 11 shows lucky image performance comparing the 22 and 90 km guide stars. It can be see that improved image quality is obtained when using 90 km guide stars. It should be noted that on the 4.2 m telescope simulated here, there is significant pupil divergence at the highest atmospheric layers even when using sodium LGSs, and hence a significant volume of turbulence remains unsampled. For larger telescope pupil diameters, the atmospheric sampling would be more complete, and better performance would be expected.

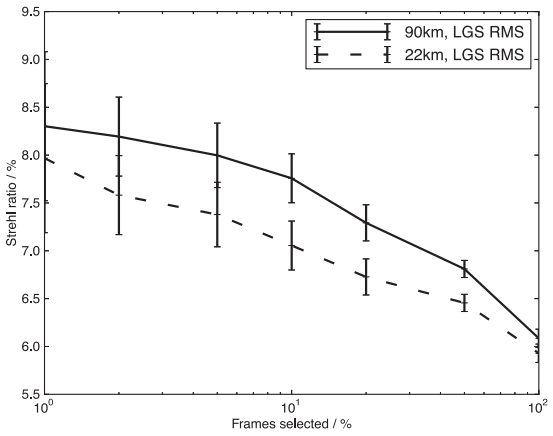

Figure 11. Lucky image quality as a function of fraction of images selected comparing a Rayleigh (22 km) and sodium (90 km) laser beacon. The long-exposure Strehl ratio is about 1.5 per cent (LGS AO with no tip–tilt corrected).

3.4 Considerations for larger telescopes

Although we have shown that the multiple LGS-assisted lucky imaging technique works well on 4 m class telescopes, it is important to consider larger telescopes, including the forthcoming Extremely Large Telescopes. The increased diameter of these telescopes (over the 4.2 m case considered here) will lead to more complete atmospheric sampling with the LGSs (due to increased cone-effect diameter), and hence improved AO correction. However, assuming that an AO system has constant pitch sub-apertures (typically 50–60 cm for current and proposed multipurpose AO systems), then as telescope size increases, the probability of AO-corrected residual wavefront phase perturbations remaining small over the whole telescope aperture decreases. Although the AO system will remove low- and mid-order wavefront perturbations (excluding tip–tilt), there is increasing probability that high-order perturbations, on scales less than a sub-aperture pitch, will remain within some parts of the pupil. Two techniques can be used to mitigate this effect:either AO system order can be increased (i.e. sub-aperture and DM actuator pitch reduced) to reduce the area of pupil over which significant unlucky turbulence remains. Alternatively, an adaptive apodization technique can be used, first detecting areas of the pupil with significant residual wavefront perturbation, and then selectively blocking these areas. However, both of these solutions introduce extra system complexity.

It should also be noted that depending on the required integrated image performance metric, small areas of residual wavefront perturbation on a large telescope pupil may not lead to a significant degradation of image quality, and therefore, the fall in probability with telescope diameter of obtaining a lucky image may be slow. Additionally, the use of LGS-only multiconjugate adaptive optics (MCAO) systems could further improve the field of view over which lucky images can be obtained, though care would be required to handle undetected 'breathing' modes of these systems.

The full extension of the proposed LGS-only AO-assisted lucky imaging technique to telescopes with 8–40 m diameters requires further study, which we do not seek to address here.

3.5 Off-axis performance

We now investigate the case where a central on-axis star is used for image centring and selection of off-axis targets (which can then

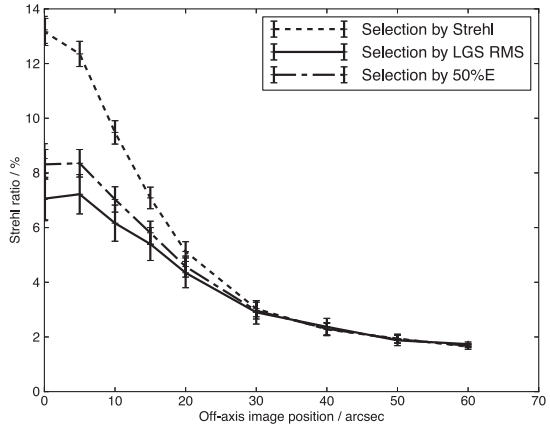

Figure 12. Off-axis performance of LGS-assisted lucky imaging, with image selection and centring performed on-axis.

be extremely faint). Fig. 12 shows performance as a function of off-axis distance (i.e. distance between the centring and selection guide star, and the science target). In the case where image selection is performed using the LGS rms wavefront error, this selection is done along the line of sight of the target, since no flux is required from the target. However, image centring is still performed using information from the on-axis guide star. This figure shows that performance falls most rapidly for selection based on Strehl ratio, and that other selection methods offer more uniform (though lower) performance across a field of view.

4 ON-SKY TESTING OF LGS-ASSISTED LUCKY IMAGING

The CANARY instrument (Myers et al. 2008) is an on-sky AO technology demonstrator, which has successfully demonstrated several different AO modes, including MOAOand tomographic GLAO, both with and without LGSs. CANARY has four Rayleigh LGSs, which are currently range-gated at a height of 22 km. It also has an AO-corrected visitor instrument port, which has previously been used for a novel spectroscopic instrument (Harris et al. 2014), and provides an ideal test-bed for developing LGS-assisted lucky imaging techniques.

We intend to use this visitor instrument port with a low-noise EMCCD to capture lucky images at high frame rate, synchronized with AO telemetry data. We will operate the lucky imaging camera using the same real-time control system that is used by CANARY (Basden et al. 2010b; Basden & Myers 2012), thus ensuring compatible data formats and time-stamping. CANARY will be operated in several AO modes during these observations, including single conjugate adaptive optics, GLAO and MOAO, with NGS-only, NGS +LGS and LGS-only modes, and we will record lucky images for both bright and faint targets so as to push lucky imaging towards greater sky-coverage. An on-axis truth WFS will be used to record on-axis wavefront phase for comparison with tomographically computed measurements. This wealth of combined AO and lucky image data will then undergo extensive post-processing to demonstrate the feasibility of full-sky LGS AO-assisted lucky imaging.

5 CONCLUSION

We have introduced the concept of tomographic LGS -assisted lucky imaging, using AO techniques to extend the use of lucky imaging for larger telescopes. We use multiple LGSs to tomographically reconstruct wavefront phase distortions due to atmospheric turbulence, and apply a correction using a DM, though without performing any tip–tilt component correction. Instantaneous images will therefore have an improved PSF, but wander about. Lucky imaging techniques are then used to select the best images, and recentre them, building up a high-resolution image. The AO correction does not require any NGSs, and thus full sky-coverage is achieved.

We have investigated the use of wavefront phase as a lucky image selection criterion, and find that it can offer improvements in image selection for cases when signal-to-noise ratio is low in the lucky images, though in the high signal-to-noise regime, conventional image selection criteria provide better selection. When field tip–tilt can be determined, this method enables lucky imaging on very faint sources.

We find that there is some advantage in reducing WFS pitch relative to DM pitch which can offer improved performance in cases when LGS flux is not limited, due to better estimation of wavefront phase. We have performed modelling with constant and variable seeing, and as expected find that lucky imaging benefits periods of good seeing within a variable seeing case, particularly when the fraction of images selected is low. We also find that using sodium LGSs can offer improved performance over Rayleigh LGSs due to increased sampling of atmospheric turbulence.

We have demonstrated that the concept of tomographic LGS-assisted lucky imaging has potential to yield near-diffraction-limited visible optical (*I*-band) images on 4 m class telescopes. Strehl ratios of up to 35 per cent have been achieved in simulations with mean seeing of about 0.7 arcsec (with a mean r_0 of 15 cm, varying sinusoidally from 10 to 20 cm). There is unlimited sky-coverage for the AO, since this concept relies only on LGS. Our simulations, which have included photon shot noise and detector readout noise, have shown that when using a crude image centring and selection criteria, stars as faint as *I*-mag 18 can be used, depending on image quality metric. On larger telescopes, fainter targets can be reached, since AO corrected, rather than seeing limited, instantaneous PSFs are used, which concentrates the photon flux into a smaller diameter core as telescope diameter increases, yielding improved signal levels. Increasing system bandpass, to increase photon flux on to the lucky imaging camera, will also increase the achievable limiting magnitude, though achromatic wide field of view optical design is non-trivial. This technique is suitable for use with all forms of tomographic AO systems, including MOAO, MCAO, GLAO and LTAO.

ACKNOWLEDGEMENTS

This work is funded by the UK Science and Technology Facilities Council, grant ST/K003569/1. The author would like to thank Richard Myers and Craig Mackay for insightful comments.

REFERENCES

Assémat F., Gendron E., Hammer F., 2007, MNRAS, 376, 287
Babcock H. W., 1953, PASP, 65, 229
Basden A. G., Myers R. M., 2012, MNRAS, 424, 1483
Basden A. G., Haniff C. A., Mackay C. D., 2003, MNRAS, 345, 985
Basden A. G., Butterley T., Myers R. M., Wilson R. W., 2007, Appl. Opt., 46, 1089
Basden A., Myers R., Butterley T., 2010a, Appl. Opt., 49, G1
Basden A., Geng D., Myers R., Younger E., 2010b, Appl. Opt., 49, 6354
Basden A. G., Bharmal N. A., Myers R. M., Morris S. L., Morris T. J., 2013, MNRAS, 435, 992

Bessell M. S., 1979, PASP, 91, 589
Ellerbroek B., Gilles L., Vogel C., 2003, Appl. Opt., 42, 4811
Femenia B. et al., 2011, MNRAS, 413, 1524
Foy R., Labeyrie A., 1985, A&A, 152, L29
Fried D. L., 1978, J. Opt. Soc. Am., 68, 1651
Garrel V., Guyon O., Baudoz P., 2012, PASP, 124, 861
Harris R. et al., 2014, Nature Commun., submitted
Law N. M., Dekany R. G., Mackay C. D., Moore A. M., Britton M. C., Velur V., 2008, in Hubin N., Max C. E., Wizinowich P. L., eds, Proc. SPIE Conf. Ser. Vol. 7015, Adaptive Optics Systems. SPIE, Bellingham, p. 70152I
Mackay C., 2013, MNRAS, 432, 702
Mackay C. et al., 2012, in McLean I. S., Ramsay S. K., Takami H., eds, Proc. SPIE. Conf. Ser. Vol. 8446, Ground-based and Airborne Instrumentation for Astronomy IV. SPIE, Bellingham, p. 844621
Morris T. J. et al., 2012, in Ellerbroek B. L., Marchetti E., Véran J.-P., eds, Proc. SPIE. Conf. Ser. Vol. 8447, Adaptive Optics Systems III. SPIE, Bellingham, p. 84470C
Myers R. M. et al., 2008, in Hubin N., Max C. E., Wizinowich P. L., eds, Proc. SPIE. Conf. Ser. Vol. 7015, Adaptive Optics Systems. SPIE, Bellingham, p. 70150E
Sivo G., Kulcsar C., Conan J., Raynaud H., Gendron E., Basden A., Vidal F., Morris T., 2014, Opt. Express, submitted
Staley T. D., Mackay C. D., King D., Suess F., Weller K., 2010, in McLean I. S., Ramsay S. K., Takami H., eds, Proc. SPIE. Conf. Ser. Vol. 7735, Ground-based and Airborne Instrumentation for Astronomy III. SPIE, Bellingham, p. 77355Z
Tubbs R. N., Baldwin J. E., Mackay C. D., Cox G. C., 2002, A&A, 387, L21

This paper has been typeset from a TEX/LATEX file prepared by the author.